ELSEVIER

25 February 1994

Chemical Physics Letters 218 (1994) 504–514

CHEMICAL PHYSICS LETTERS

Femtosecond dynamics of coherent photodissociation–recombination of I_2 isolated in matrix Ar

R. Zadoyan, Z. Li, P. Ashjian, C.C. Martens, V.A. Apkarian

Department of Chemistry, University of California, Irvine, CA 92717-2025, USA

Received 20 October 1993; in final form 23 December 1993

Abstract

Pump–probe studies of I_2 in matrix Ar, with a time resolution of 180 fs, are reported. The experiments are simulated using classical molecular dynamics. Dissociative excitation of $I_2(A)$ results in coherent cage-induced recombination on the A/A′ surfaces. The recombinant molecule vibrates coherently even after extensive energy loss.

1. Introduction

Studies of the photodissociation of a diatomic molecule allow the description of one of the most fundamental processes in chemistry, namely, the cleavage of the chemical bond. In condensed media, the separation of photofragments is subject to hindrance by the immediate solvent, a process that has come to be known as the cage effect. The cage effect has accordingly become the central theme in condensed phase photodissociation studies. The effect is expected to be most pronounced in the rigid lattices provided by the solid state.

Although detailed descriptions of photodissociation in rare-gas solids have in recent years become available through molecular dynamics simulations, to date, experimental studies of these model systems have been limited to time-independent measurements proving the consequences of caging [1]. Direct, time-resolved observations of caging have only recently become available in the rather special system of I_2^- in polar clusters [2]. In an elegant set of experiments on I_2^- encased in size-selected clusters of CO_2, recombination with coherence lasting several picoseconds was observed for states that in the absence of a complete cluster cage would have been purely dissociative [2]. In contrast, in the case of neutral I_2, which as the prototype of condensed phase photodissociation dynamics has the longest record of experimental scrutiny, such coherences in the liquid phase are absent [3]. The media in which the time-resolved studies of I_2 have been carried out, liquids [3] and clusters [4], evidently provide only a *soft* cage, which induces too much vibrational dephasing of the evolving I_2 to yield lasting coherences.

Most recently Liu et al. have carried out measurements with femtosecond resolution in large Ar clusters, which reveal that, when $I_2(A)$ is prepared on its repulsive wall, in addition to the signal resulting from the first passage of the wavepacket through the probe window, coherent recoil from the cage and recombination occurs [5]. The experiments in solid Ar that we report are carried out under very similar conditions. In the extended solid, persistent coherent oscillations are observed after photodissociation–recombination.

We report the first observation of coherent recombination dynamics of I_2 following photodissociation

SSDI 0009-2614(94)00035-0

in solid Ar, together with theoretical modeling of the experiment by molecular dynamics simulation. In view of the extensive prior work on I_2, our studies allow direct comparisons of the same dynamics in different many-body environments: clusters, liquids, and solids. In this regard, particularly useful are the recent studies of Lienau et al. along the gas–liquid transition region, which serve to directly link the dynamics of the isolated molecule to that in condensed media [6].

2. Experimental

The experiments consists of pump–probe measurements conducted on I_2 isolated in matrix Ar. The matrices are prepared by spraying premixed gaseous samples of I_2:Ar (1:5000) on a 0.5 mm thick sapphire window held at 15 K. Using an adjustable leak-valve, deposition conditions have been adjusted to produce transparent films of high optical quality. The ultimate time response of pump–probe experiments in these films is determined by multiple scattering.

The light source consists of a cw mode-locked Nd:YAG laser (Coherent Antares 76), which is frequency doubled to synchronously pump a dispersion compensated femtosecond dye laser (Coherent Satori). For operation in the 700–740 nm range, pyridine 1 is used as the gain medium and DDI is used as the saturable absorber. Autocorrelation of the dye laser pulses typically yields a pulse width of 150 fs fwhm. A small fraction of the YAG fundamental is picked off and amplified in a regenerative amplifier (Continuum RGA60), operating at 30 Hz. The doubled output of the RGA is used to pump a dye amplifier, to amplify the femtosecond pulse energies up to ≈ 0.5 mJ. The amplified dye pulses are split into two beams. One of the beams is used as the pump source in the experiments. The second beam is doubled in a 1 or 0.5 mm BBO crystal to produce UV probe pulses of ≈ 10 μJ energy. The time resolution of the system, as measured by difference frequency generation in a nonlinear crystal, is ≈ 250 fs fwhm when the 1 mm doubling crystal is used. With the shorter crystal, and using a 0.2 mm BBO for difference generation, cross-correlation widths of ≈ 180 fs are obtained.

The absolute position of $t=0$ and the response function of the system are important parameters in the analysis of the data. Accordingly, the cross correlation between pump and probe pulses is recorded along with the signal (fluorescence intensity as a function of delay between pump and probe). Matched windows are used to produce identical dispersion in the beam paths past the beam splitter. The only residual difference between the two legs is the differential dispersion between the thin film sample (≈ 30 μm), and the crystal of the cross correlator. In the difference generation geometry, BBO has a negative dispersion, while we expect normal dispersion in our sample. Accordingly, there is an effective retardation of the cross correlation relative to the true origin of time. Based on its known optical properties, for the 0.2 mm thick BBO crystal, a delay of ≈ 80 fs is to be expected on the measured $t=0$ [7]. Even if we correct for this dispersion, an estimated uncertainty of ≈ 50 fs remains in the determination of the absolute origin of time. No corrections are made in the data to be presented.

3. Results

In the experiments to be described, I_2 is excited in the spectral region between 628 and 734 nm. This corresponds to access of the repulsive wall of the $A(^3\Pi_{1u})$ state, in an energy window spanning from above the molecular dissociation limit to just below the $B(^3\Pi_0)$ potential minimum. In addition to the nested A and A′ states, several shallow electronic states are known to exist in this range of energies [8]. There is significant uncertainty in the details of the molecular potentials in the matrix environment. Analysis of vibrationally relaxed emission on the $A \rightarrow X$ and $A' \rightarrow X$ transitions are the main sources of the spectroscopic characterization in matrices [9–11]. The electronic origins of A and A′ are shifted by ≈ 250 cm^{-1} relative to the gas phase [11], and their equilibrium distances are shifted by ≈ 0.01 Å [10] (or less [#1]). With the assumption of the gas phase molecular dissociation limit, it can be inferred that A and A′ are bound by 1890 and 2730 cm^{-1}, respectively. Using these binding energies, the gas phase equilibrium distances and harmonic frequencies [12], Morse functions can be constructed to repre-

[#1] See discussion of reanalysis in ref. [11].

sent the potentials. These are shown in Fig. 1.

The time evolution of the system is probed with the second harmonic of the pump pulse, by monitoring laser-induced fluorescence from the lowest ion-pair state, the D′ (2_g) state. This emission has previously been observed and assigned in matrices by Macler and Heaven [11]. It occurs at 382 nm in Ar, significantly shifted from its gas phase origin of 340 nm [13]. The red-shift can be understood in terms of solvation of the ionic upper state in the polarizable host. Little else is known experimentally about the solvated ion-pair states. We expect the six lowest of these states, which correlate with $I^-(^1S)+I^+(^3P)$ and have very similar energetics in the free molecule, to be strongly coupled and overlapped in the solid. In addition to D′, this manifold should contain the $\beta(1_g)$ state. If the gas phase propensity of $\Delta\Omega=0$ is maintained for covalent to ion-pair transitions, then the probe radiation may induce both $\beta\leftarrow$A and D′$\leftarrow$A′

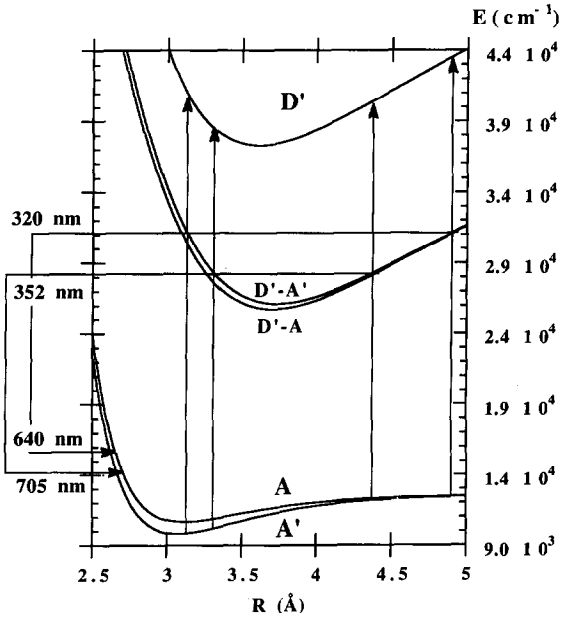

Fig. 1. A partial potential energy diagram of I_2. The A($^3\Pi_{1u}$) and A′($^3\Pi_{2u}$) curves are given as Morse functions, based on their matrix-shifted electronic origins, and gas phase dissociation limits. The D′ state is directly taken from the gas phase, and vertical lowered to reproduce the experimentally observed D′$\rightarrow$A′ emission peak at 382 nm. Also shown are the difference potentials, D′$-$A′ and D–A. The latter are double valued at all probe wavelengths, as indicated by the crossings with the horizontal lines. Two windows are simultaneously probed at each wavelength.

excitations [14]. Both transitions are expected to lead to the same emission, namely, emission from the vibrationally relaxed lowest ion-pair state: D′$\rightarrow$A′. In short, while the pump predominantly prepares population on the A surface [#2], both A and A′ states are probed. We rely on the vertically shifted gas phase D′ potential to represent the lowest ion-pair manifold, and make estimates of expected resonances on this basis. The D′ potential, in its Rittner form [15], is shown in Fig. 1. Also shown are the D′$-$A′ and D′$-$A difference potentials, which according to the Franck principle dictate the probe resonances. The difference potential are double valued at all experimental probe wavelengths. Accordingly, two resonances are expected at each wavelength, both on the attractive limb of the A/A′ surfaces. We indicate in Fig. 1 the expected pumped and probed configurations at two different wavelengths. Note that in the case of the 640+320 experiments, the outer probe window stretches as far out as $\approx$5 Å, and therefore interrogates configurations where the effective cage wall is to be expected. It should be emphasized that the construct of Fig. 1 is only an a priori estimate of potentials, to be used as an initial guideline. We expect that the time-resolved measurements, together with theoretical modeling, will enable a finer tuning of these potentials, especially on the stretched molecular configurations which cannot be probed by standard spectroscopic techniques.

The time profiles of the signals obtained with an experimental response time of 250 fs (fwhm of cross correlation) at different wavelengths are presented in Fig. 2. The time evolution in the first 4 ps is shown in the inset. In this range of excitations, the molecule is prepared at excess energies (energy above the dissociation limit of I_2), ranging from 3500 to 1000 cm^{-1}. For short excitation wavelengths, the signal reaches a plateau after peaking. The plateau-to-peak ratio diminishes as a function of wavelength, and beyond 700 nm the plateau disappears. This is a result of the inner probe window moving out of the $v=0$ resonance on the A/A′ states. According to the difference potential of Fig. 1, between 640 and 730 nm, the inner resonance moves from 3.1 to 3.36 Å. The

[#2] Based on radiative lifetimes of A($v=0$) and A′($v=0$) in Ar [9], it can be estimated that the absorption strength of A$\leftarrow$X transition is $\approx$350 larger than that of A′$\leftarrow$X.

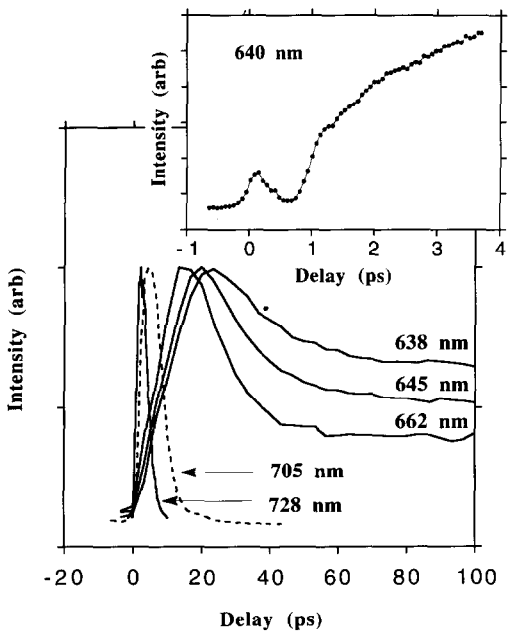

Fig. 2. Fluorescence of the ion-pair state as a function of delay between pump and probe pulses. The pump wavelengths are indicated, the probe wavelength is always the second harmonic of the pump. The signals are normalized to the same height. The inset shows the first 4 ps evolution of the signal, recorded with an experimental response time of 250 fs. In this time scale, nearly identical signals are obtained between 638 and 662 nm.

resonance window therefore moves from near the maximum of the $v=0$ wavefunction ($r_e(A')=3.07$ Å and $r_e(A)=3.1$ Å) to well outside it. The signal peak corresponds to buildup and decay of Franck–Condon intensity at interatomic distances probed by the inner window. A simple kinetic analysis of these time profiles is not possible. A dynamical analysis, which accounts for the time evolution of Franck–Condon probabilities at the probe resonances is required, as will be shown below. Qualitative trends are, however, clear. As the probe window moves out on the attractive limb of the potential, the peak develops at earlier times. The time constant of 12 ± 2 ps, which fits the fall time of the transients at short wavelengths, can be associated with the time scale of complete vibrational relaxation within the A/A′ manifold. The early time behavior, inset to Fig. 2, shows a peak which occurs within the uncertainty of the time origin and reflects the experimental response (≈ 250 fs in this case). The signal, after dropping to the background level, builds up nearly a picosecond later. This signal quite closely resembles the observations in large Ar clusters [5]. The first peak corresponds to passage of the initially prepared wavepacket through the probe window, and the recursion corresponds to coherent recoil of the atoms from the cage wall. The subsequent signal growth occurs in a stepwise fashion; this, however, is a very weak effect at this excess energy, and is poorly resolved with the 250 fs time response.

It should be noted that, in these experiments, no permanent dissociation of I_2 occurs. This is verified by the constancy of the pump–probe signal after several days of irradiation of the sample, and by the absence of any accumulation of product I atoms. Caging is complete in solid Ar at all studied excitation wavelengths, which have already been extended to the spectral range of 730 to 480 nm.

The early time profile of the signals was recorded with an experimental resolution of 180 fs (fwhm of cross correlation). These are shown in Fig. 3, where clear oscillations can be observed over a growing

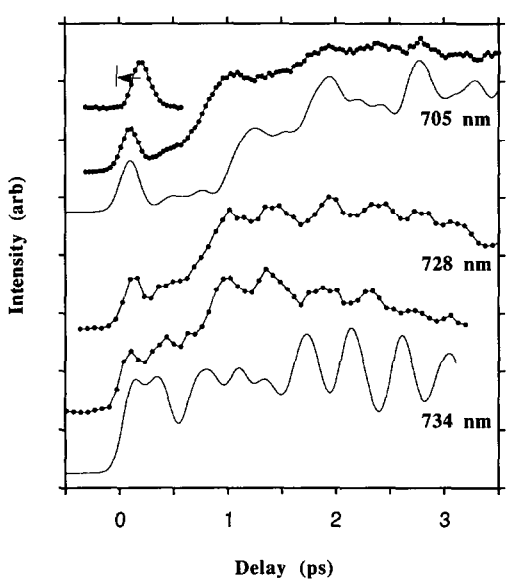

Fig. 3. Coherent recombination and relaxation dynamics observed at early time, with an experimental resolution of 180 fs. The data at 705 and 734 nm are compared to the theoretical signals calculated from the simulated classical trajectories (solid lines), using 20 trajectories in each case. Also shown is the cross correlation, which, due to the additive dispersions between sample and the correlator crystal, is retarded relative to the signal. The estimated correction of the time origin is indicated with the arrow.

background of signal. The oscillations are an indication that the recombination and subsequent vibrational relaxation in the bound part of the potential proceeds by maintaining significant coherence in the population, with the time-spread in the wavepacket shorter than the vibrational period of ≈ 0.5 ps of the I_2 molecule. There are clear wavelength-dependent trends with respect to the depth of the modulations and their recursion times. It is evident, for example, that the persistence of the oscillations is longer at the lower excitation energies. Comparison of the 705 nm response with that of 728 nm also shows that, while effective recursion times of 1 ps are observed in the former case, in the latter case the oscillation frequency has doubled, leading to a recursion time of ≈ 0.5 ps. Another aspect of the wavelength dependence is that intensity develops between the first peak and the first recurrence (the first 1 ps period) as the excitation energy is lowered. In this time interval, while at 640 nm the signal intensity drops to the background level (see inset in Fig. 3), at longer wavelengths the intensity gradually builds up. Based on the potentials of Fig. 1, it is clear that both probe windows contribute to the observable signal at early time; accordingly, detailed interpretations should be made with care.

Given the fact that 10 electronic surfaces correlate with the $I(P_{3/2})+I(P_{3/2})$ asymptote, and that the recombination and subsequent relaxation occurs on (at least) a pair of nested electronic states, it is quite impressive to observe coherences that last several vibrational periods. The robustness of the mechanics is presumably due to the similarity of the nested A and A′ surfaces. Accordingly, it could be expected that a single surface classical simulation would capture at least the qualitative essence of the observed dynamics. We have performed such simulations, and use the results as a framework for the interpretation of the experiments.

4. Simulations

Molecular dynamics calculations were performed using a lattice of 512 Ar atoms, with one I_2 molecule occupying a doubly substituted site in the center of the simulation box. All interactions are assumed to be pairwise additive. For the I_2 potential we use a Morse function representative of the A state. For I–Ar we employ Lennard-Jones parameters derived from Xe–Ar interactions. The Ar–Ar interactions are also represented by a potential of the Lennard-Jones form. The pair potential parameters are collected in Table 1. The system is first equilibrated at 15 K using the $I_2(X)$ state parameters. Initial configurations are randomly chosen from the equilibrated set with the condition that $r(I_2)$ correspond to the desired Franck–Condon resonance condition for a given wavelength of excitation to the A state. The I_2 potential is then suddenly switched to $I_2(A)$, and Hamilton's equations are propagated in time using standard integration methods. The resulting time dependence of the I_2 separation for each member of an ensemble of trajectories, and total ensemble averaged I_2 vibrational energy are shown in Fig. 4. After an initial extension to 4.5 Å, the trajectories collide with the Ar cage, are decelerated, and return to the inner turning point of the molecule at $t \approx 1$ ps. The ≈ 150 fs spread in arrival times to this configuration, represents the dephasing time of the classical trajectories. Approximately 70% of the initial energy is lost upon the first collision. This quantity closely corresponds to the expected energy loss resulting from a head-on binary collision between atomic iodine and Ar: $|\Delta E/E| = 4m_I m_{Ar}/(m_I + m_{Ar})^2 = 0.73$. Despite this agreement, the collision with the cage is a complex process; analysis of the classical trajectories indicates that multiple collisions occur among atoms in different shells prior to recoil of the I_2. The effective cage potential can be extracted from the recoil distance as a function of initial excess energy. At excess energies of 1000, 1700, and 2700 cm^{-1}, the recoil distances are 4.45 ± 0.25, 4.9 ± 0.25 and 5.25 ± 0.25 Å, respectively. Although still above the dissociation

Table 1
Potential parameters used in the MD simulations

Potential parameters	Values
E_3	1840 cm^{-1}
r_e	3.10 Å
β	2.147 $Å^{-1}$
ϵ_{Ar-Ar}	83.26 cm^{-1}
σ_{Ar-Ar}	3.405 Å
ϵ_{I-Ar}	130.24 cm^{-1}
σ_{I-Ar}	3.617 Å

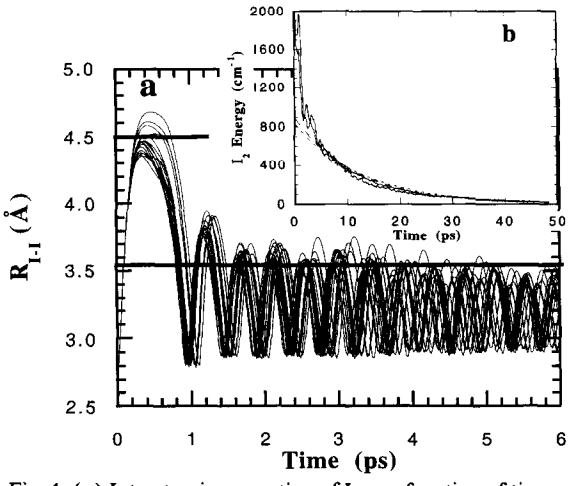

Fig. 4. (a) Interatomic separation of I_2 as a function of time, as obtained from the molecular dynamics simulations. Initial excess energy in this case is 1000 cm^{-1}, which closely corresponds to the experimental excitation at 734 nm. The horizontal lines correspond to the probe windows used in the theoretical calculation of the time-dependent signal from the trajectories, for comparison with experiment in Fig. 3. (b) The sum of potential and kinetic energies in I_2 as a function of time. The two curves are the average of twenty trajectories each, generated at initial excess energies of 1700 and 1000 cm^{-1}. Also shown as dashed lines are the exponential fits, which yield a time constant of 12 ± 1 ps for vibrational relaxation. The first-order decay fits the data for $t > 4$ ps. At $t < 4$ ps, the energy loss occurs in steps, with $\Delta E/E \approx 0.7$ for each effective collision, in good agreement with a simple collisional energy transfer model.

limit, in the second stretch the molecule can only reach a separation of ≈ 3.8 Å, and remains within the bound part of the molecular potential. Subsequently, the I–I bond undergoes damped oscillations with a period of ≈ 0.5 ps. It can be seen in the inset to Fig. 4 that the energy loss in the first ≈ 4 ps is dominated by step functions, while at longer times an approximately exponential decay, independent of initial energy content, is observed. The exponential fit at long time, shown in Fig. 5, yields a decay constant of 12 ± 1 ps for vibrational relaxation, in excellent accord with the fall time extracted from the experimental decay.

To make a direct comparison of the simulation with experiment, the trajectories are converted to signal using the classical reflection principle. Treating the ensemble of trajectories as a time-dependent probability in position, $\rho(R, t)$, where R is the I–I bond length, an absorption occurs at the probe wavelength when $\Delta V(R) = h\nu$. The time-dependent signal $S(t)$ is thus given by

$$S(t) \propto \int |\mu_{if}(R)|^2 \rho(R, t) \delta(\Delta V(R) - h\nu)\, dR , \tag{1}$$

in which μ_{if} is the R-dependent electronic transition dipole, and $\delta(\Delta V(R) - h\nu)$ is an energy-conserving Dirac delta function at the resonance condition $\Delta V(R) = h\nu$. For the experimental wavelengths employed, this condition has two roots R_j ($j = 1, 2$), which in turn depend on the laser wavelength. Performing the integration over R and using well-known properties of the delta function, the signal becomes

$$S(t) \propto \sum_{j=1}^{2} \frac{|\mu_{if}(R_j)|^2 \rho(R_j, t)}{|\partial \Delta V(R_j)/\partial R|} . \tag{2}$$

For an ensemble of N trajectories, the evolving probability density $r(R, t)$ is given by

$$\rho(R, t) = \frac{1}{N} \sum_{n=1}^{N} \delta(R - R_n(t)) , \tag{3}$$

where $R_n(t)$ is the instantaneous position of the nth member of the ensemble. To represent $S(t)$, the terms $\delta(R - R_n(t))$ need to be replaced by analogous functions of time. Defining $t^*_{n,k}$ as the kth time at which the nth member of the ensemble satisfies a resonance condition ($R_n(t) = R_1$ or $R_n(t) = R_2$), the time-dependent signal can be written as

$$S(t) \propto \frac{1}{N} \sum_{j=1}^{2} \frac{|\mu_{if}(R_j)|^2}{|\partial \Delta V(R_j)/\partial R|} \times \sum_{n=1}^{N} \sum_{k} \frac{1}{|v_n(t^*_{n,k})|} \delta(t - t^*_{n,k}) . \tag{4}$$

Here, the factors $|v_n(t^*)|$ appearing in the denominator are the absolute velocities of the ensemble members at the resonance times t^*, and result from the position to time variable change in the delta functions. The result is a sampling function, which corresponds to a set of delta functions in time. In addition to the R-dependent electronic transition dipole, the delta function signals are also weighted by the derivative of the difference potential at a particular window (density of states) and by the velocity of the trajectory at the crossing of the window (dwell time). This purely classical treatment fails at turning points, where the velocity $v \to 0$, and also for values of R for

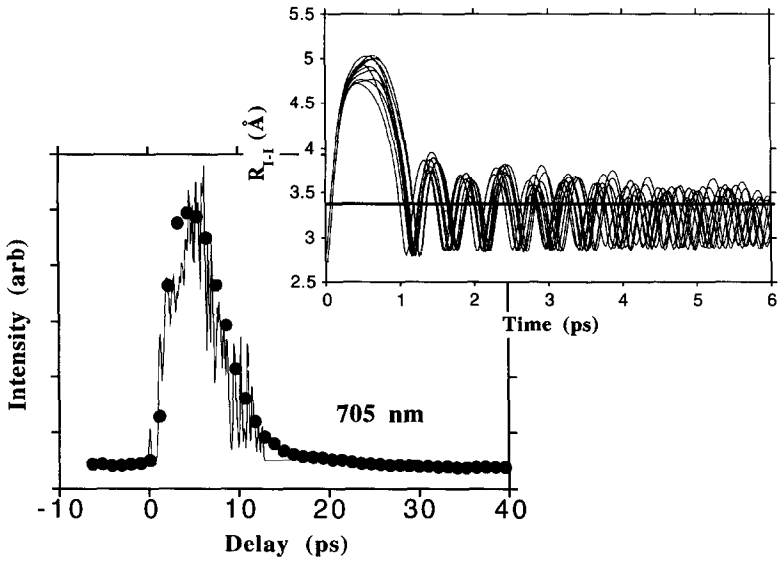

Fig. 5. Fit of the long-time profile of the 705 nm data to the theoretical predictions, which was generated from the classical trajectories shown in the inset. The window used in the simulation, $R_1 = 3.42$ Å, is also shown in the inset. The oscillations in the simulated signal at long time is an artifact of singularities encountered at the crossings of the window with turning points of the classical trajectories.

which the initial and final states are parallel. It should be obvious from the difference potentials in Fig. 2 that the latter condition does not arise in the present. To overcome the infinities encountered at turning points, an approximate uniformization is employed, where the zero-point uncertainty is included in the velocity weighting, yielding

$$S(t) \propto \frac{1}{N} \sum_{j=1}^{2} \frac{|\mu_{if}(R_j)|^2}{|\partial \Delta V(R_j)/\partial R|} \times \sum_{n=1}^{N} \sum_{k} \frac{1}{\sqrt{v_n^2(t_{n,k}^*) + 2\hbar\omega_0/\mu}} \delta(t - t_{n,k}^*) \,. \quad (5)$$

The resulting set of delta functions in time are then convoluted with the experimental response function, as obtained from the cross correlation signal.

5. Discussion

The fit of $S(t)$ to the long-time transient for 705 nm excitation is shown in Fig. 5, together with the trajectories used in the simulation. Reproduction of the overall signal envelope, which is primarily determined by the inner probe window, is sought in such a comparison. At a value of $R_1 = 3.42 \pm 0.03$ Å, which is consistent with the potentials of Fig. 1, an acceptable fit is obtained. The indicated error is a reflection of the sensitivity of the fit to the choice of R_1. The sensitivity of this analysis can be discerned by noting that the signal duration is a measure of the time at which the oscillation amplitude of the trajectories fall below the observation window. It should also be noted that the classical inversion of the trajectories produces artificial oscillations at long times, where turning points of the trajectories pile up. This is to be expected as a failure of the quantum/classical correspondence in the treatment, which becomes most severe at long times and at turning points. The zero-point energy contribution in Eq. (5) is generally found to be insufficient to damp the oscillations at turning points.

Inspection of the ensemble of trajectories in Figs. 4 and 5 provides clues to the expected signals at early time. With a single probe window, the first passage of the trajectories through the resonance should produce a peak in time. This should be followed by a silent period of ≈ 1 ps, after which the trajectories return to the resonance window and produce subsequent oscillations. These features are contained in the data. However, the experiments also show a signal that contributes in the first 1 ps period, which be-

comes more prominent as the excitation wavelength is increased. The latter could only result from the second resonance, from the outer window. Moreover, to yield signal at ≈ 0.5 ps, the outer window should be situated near the cage wall. This consideration is used in the construction of signals from the simulations: the inner probe window is chosen from the fit to the long-time profile, while the outer window is chosen to fill in the silent period to match with the experiment. With an inner window of $R_1 = 3.42$ Å, the 705 nm data are reproduced by choosing an outer window of $R_2 = 5.1$ Å. In adding the contributions from these well separated windows, the ratio of transition dipoles $|\mu_{if}(R=5.2)|^2/|\mu_{if}(R=3.42)|^2 = 0.3$ is used. The comparison between simulation and experiment is shown in Fig. 3. From the inset to Fig. 5, it should be clear that few trajectories fall in this outer window – the outer reaches of the cage wall is being observed. The trajectories illustrated in Fig. 4 are used to simulate the 734 nm data. An inner window of 3.55 Å and an outer window of 4.5 Å are used, and these contributions are added with the assumption of equal transition dipoles. The comparison is shown in Fig. 3. The exaggerated oscillations past 2 ps in the simulation is an artifact, and is due to the sampling of the turning points of the classical trajectories. This is another indication that the damping scheme used in Eq. (5) is not quite satisfactory. Given the inherent approximations in the treatment, and uncertainties in the solvated potentials, the gross features of the data seem acceptably reproduced. The choices of R_1 and R_2 would imply that the equilibrium distance of the solvated ion-pair potential has stretched by ≈ 0.2 Å in Ar. Such a shift is consistent with the expectation that, due to the dielectric of the medium, the Coulombic attractive wall of the potential should be softened.

Several aspects of the comparison in Fig. 3 are notable. At 705 nm, the prominent peaks in the experiment show an interval of ≈ 1 ps, despite the fact that the vibrational period of $I_2(A/A')$ is ≈ 0.5 ps. The theoretical treatment reproduces this behavior, although the simulation shows larger dips between the peaks. The period doubling of the coherent oscillations at higher excess energy can be understood by careful examination of the simulations, and are seen to arise from the collective molecule–cage dynamics: the higher excess energy at 705 nm leads in turn to a larger collisional excitation of the local vibrations of the Ar cage atoms along the I–I axis. The cage then coherently expands and contracts during the first several I_2 vibrational periods, with a definite phase relation to that of the oscillating diatomic. During the contraction of the cage, the I_2 vibrational amplitude is diminished by repulsive interactions with the collinear Ar atoms. As the cage expands, the steric repulsion is relieved, and the I–I bond extension can be larger. The result, which is illustrated by the trajectory ensemble shown in Fig. 5, is an oscillation in the maximum I_2 amplitude, with a characteristic period of ≈ 1 ps. This effect is observed to persist for several vibrational periods (around 3 ps), and when combined with the classical reflection simulation of the time-dependent signal, leads to the 1 ps period oscillation in the measured signal. The role of coherent motion of localized "bath" modes in nonstatistical decomposition of $I_2(B, v)$–Ar_{13} clusters have been previously examined from the perspective of molecular dynamics simulation, and the possibility of such effects in condensed phases has been discussed [16].

In contrast with the 705 nm data, at longer wavelengths, oscillations with a period of ≈ 0.5 ps persist quite regularly for times as long as 6 ps. This is reproduced by the simulation, although there seems to be a phase shift between experiment and theory for $t > 1.5$ ps (see 734 nm data in Fig. 3). There is now a peak at 1.5 ps in the experiment, where there was none in the 705 nm data (Fig. 3). The effect of the cage recoil is washed out at the lower energy, as seen in both experiment and simulation.

There are several discrepancies between simulation and experiment that require comment. In the 705 nm case, it is evident that the duration between first passage of the wavepacket from the inner observation window and its first return is shorter in the experiment by ≈ 200 fs, yet the positions of the later maxima agree relatively well. A shorter recoil time could be expected if the true I–Ar potential were significantly more repulsive than the model potentials used here. However, a shorter recoil time would advance the entire simulated trace and would therefore spoil the agreement among the delayed peak positions. A more consistent explanation may be found in the consideration that the molecule recombines on the nested pair of A/A′ potentials. It can be seen in the difference surfaces of Fig. 2 that this results in

further splitting of the inner window into two, by 0.1–0.3 Å, with the A′ window stretched farther out than the A window. In the outgoing trajectories, the system evolves on the A state where it was initially prepared. After recoil, if a significant portion of the population returns on the A′ surface, then an earlier signal would be expected due to the location of the A′ probe window. Subsequent oscillations would proceed on both surfaces, and therefore the positions of the later maxima would be retained. The presence of coherently oscillating populations on two surfaces could also bring a closer agreement between simulation and experiment by filling in the deep valleys of the simulated signal. The latter effect, the difference in depth of modulation between simulation and experiment has another obvious source: the neglect of zero-point amplitude in the classical simulations. At the cryogenic temperatures of these experiments, the zero-point energy of the lattice is comparable to the thermal energy. We have recently demonstrated that the neglect of zero-point amplitudes can at least partially be remedied by carrying out simulations at scaled temperatures, bringing experiment and simulation in closer agreement [17]. These considerations are generally applicable to the present treatment of the data, and could be argued to be also responsible to the discrepancies between experiment and simulation at 734 nm.

The general issue that many electronic states can potentially take part in the dynamics, yet a single surface simulation seems to adequately capture many of the features of the observed signals, requires closer scrutiny. We have assumed that both A and A′ are visible by the probe, and it is known that population is efficiently exchanged between these two nested potentials [9,10]. The energy exchange is assumed to be most effective on the attractive part of the potentials, in the highly vibrationally excited states where the adiabatic transfer can occur with single-phonon energy gaps, and with favorable Franck–Condon factors [10]. Evidently, this process does not produce a significant dephasing to destroy the coherence in the oscillating populations, at least at low excess energies. The possibility of non-adiabatic energy transfer on the repulsive wall, immediately after preparation of the wavepacket, also exists. Such a mechanism has been advanced in the gas phase [18], between $B(^3\Pi_{u0})$ and the $^1\Pi_{1u}$ surfaces, in order to explain the observed one-atom cage effect [19]. In the present, such a transfer would split the wavepacket, creating a significantly slower fragment on the A′ repulsive wall after the sudden loss of $\approx 1500\ cm^{-1}$ to the lattice. This process is however quite unlikely in the solid, since it would involve the sudden creation of more than 20 phonons simultaneously.

Somewhat surprisingly, we find no evidence for the participation of the ground state in the dynamics. Crossing over to the X state should lead to permanent loss of signal. Yet the comparison between experiment and simulation shows no such loss. In principle, population on the X state could be observed via a D←X resonance, at wavelengths shorter than the D′←A′ resonance. Yet, no such contribution is observed, especially in the long-time scans at short wavelengths (Fig. 2), where instead of a long-term transient characteristic of vibrational relaxation on the X surface, population accumulation in $v=0$ of the A/A′ states is observed. The transfer from A/A′ to X corresponds to a Π to Σ flip, which would be induced by the angular anisotropy of the I–Ar pair interactions. Such non-adiabatic dynamics in the solid lattice has recently been treated by simulations [20]. For collinear collisions, an earlier cage wall is to be expected for Π interactions as compared to Σ. At the present excitation energies, it may be the case that the molecule does not reach a large enough separation to experience the convergence of these surfaces where non-adiabatic transitions become possible.

6. Conclusions

In this Letter, we have reported the first time-resolved studies of a solid state photodissociation–recombination process. The experimental results were analyzed by comparison with theoretical predictions generated by molecular dynamics simulation, combined with a simple classical reflection model to translate trajectory data into time-dependent signals. While the treatment is approximate, it succeeds in capturing the essence of the experimental observations. Given the demonstrated experimental detail, systematic theoretical treatments including non-adiabatic effects would be highly desirable in future investigations of this model system. The experimental detail could be significantly enhanced by the use of

independent pump and probe wavelengths. This is particularly needed since there is significant uncertainty in the solvated potentials of I_2. Despite these shortcomings, these initial studies allow us to draw important conclusions about the solid state dynamics, and allow comparisons of the main results with those obtained for liquids and clusters.

The caging of I_2 is complete in solid Ar. The process, including the direct observation of the molecule–cage collision, is most directly monitored in the present experiments. The cage-induced recombination of the I atoms proceeds coherently, and leads to oscillations of the nascent molecule in the lattice with a population coherence that lasts for several vibrational periods. The lower the initial excess energy, the longer is the persistence of coherence, which lasts even after extensive vibrational energy loss to the lattice. This suggests that the origin of dephasing is the cage recoil, which is set in motion by the initial collisional agitation of the lattice. Further, it has to be concluded that the system retains memory of the initial excitation for periods of several picoseconds. Direct feedback of the cage on the guest atomic motions is also observed in the form of a period doubling in the oscillations of the time-dependent signal as excess energy is increased. In contrast, the vibrational relaxation rate is independent of initial excitation energy. It is determined by the mechanical couplings, which, given by the agreement between simulation and experiment, are well reproduced by the assumed potential parameters. The retention of coherence for many vibrational periods is the key to creating the oscillatory signals observed in the present study. Coherences in reactive dynamics that last several vibrational periods are of great interest, since they imply that, with proper choice of systems, chemical reactions in condensed media may proceed with mechanical specificity, relatively unaffected by random dephasing induced by interaction with the bath modes.

The present results can be directly compared with the recent studies of I_2 entrapped in large Ar clusters [4,5]. In the clusters, coherent cage-induced recoil of I_2 is observed; however, at the reported excitation wavelengths, subsequent coherences in the nascent I_2 population is washed out [5]. Extension of the cluster studies to longer wavelengths would be highly useful in assessing whether at softer collisions coherence can be maintained in the recombinant molecule. The observed recombination time in the clusters appears to be shorter than what is observed in the solid. However, this comparison should be made with great care, since the probe windows in the two cases can be dramatically different. This is due to the strong solvation of the ion-pair state, which dictates the probe resonance location, and therefore a strong sensitivity of the probe window to structure and size of the clusters is to be expected. In the clusters, there is clear evidence of extensive cage exit and subsequent diffusion-controlled recombination [4], while caging is complete in the case of the solid. We have verified that while coherence is lost, caging remains complete in the solid even when I_2 is initially prepared at excess energies of ≈ 1 eV. It is also believed that, in the clusters, recombination on the ground state is observed [5]. The arguments for the latter conclusion are not compelling, but not unexpected. Adiabatic transfer from A/A′ to X is to be expected if the atoms exit the cage. That we see no evidence of this process in the solid we attribute to the separation between the Σ and Π repulsive walls, and surmise that at the excess energies in the present studies the convergence between these two surfaces is not reached. The arguments leading to our conclusion do not obviate the presence of a small channel for conversion to the ground state.

The dynamics observed in solid Ar is more closely reminiscent of the photodissociation–recombination dynamics of I_2^- in small clusters of CO_2 [2]. Although recorded with a longer time resolution, the recombination there shows oscillations that span several vibrational periods. Evidently, the charge–dipole interactions create a cage that is significantly tighter than in the case of neutral clusters, and comparable to the cage experienced by the molecule in the extended solid. In recent time-resolved studies, coherent oscillations in I_2^- generated by photodissociation of I_3^- in polar solvents has been observed [21,22]. These are quite relevant to the general understanding of dephasing and relaxation dynamics in condensed media, but differ from the present case in their origin. In the photodissociative generation of I_2^-, the coherence is transferred from the parent in its impulsive dissociation, in the case of coherence built by photodissociation–recombination, the dynamics is dictated by the initial fragment–solvent interactions. The suddenness of the first collision, and a small het-

erogeneous contribution to the cage distribution, are crucial in retaining coherence in the subsequent vibrational relaxation of the reformed molecule.

The extensive studies carried out on I_2 in the liquid phase have shown no real evidence of coherent recombination dynamics. Zewail et al. have reported on a liquid phase measurement under very similar conditions to the present studies (excitation of I_2 (A) in liquid CCl_4 at 620 nm and probing via ion-pair state excitation) [23]. Although recombination starting within 200 fs of the initial excitation is reported, the signal builds up with a rise time of 5 ps, and a dephasing time of 200 fs is inferred [23]. In their recent work on CH_2I_2, the Harris group also concludes that single collision-induced recombination does proceed in $\approx$350 fs in the liquid phase [24]. In general, however, this pertains to a sub-ensemble of the molecules. The combined effects of structural disorder and a much softer cage presumably produce a large distribution in recombination times, stretching from single collision-induced events, to much longer lasting diffusion-controlled recombination [3]. This is consistent with the relative success of treatments of the liquid phase process by dissipative stochastic dynamics [25]. In contrast, the solid provides an ordered rigid cage, in which sudden dynamics predominates.

7. Acknowledgement

VAA acknowledges support by the US Air Force Phillips Laboratory under contract S04611-90-K-0035 and AFOSRF49620-1-0251. CCM acknowledges support from the National Science Foundation and the Office of Naval Research. We also acknowledge the UCI Office of Academic Computing for an allocation of computer resources.

8. References

[1] M. Chergui and N. Schwentner, Trends Chem. Phys. 2 (1992) 89.
[2] J.M. Papanikolas, V. Vorsa, M.E. Nadal, P.J. Campagnola, J.R. Gord and W.C. Lineberger, J. Chem. Phys. 97 (1992) 7002, and references therein.
[3] A.L. Harris, J.K. Brown and C.B. Harris, Ann. Rev. Phys. Chem. 39 (1988) 341, and references therein.
[4] E.D. Porter, Q. Liu and A.H. Zewail, Chem. Phys. Letters 200 (1992) 605, and references therein.
[5] Q. Liu, J. Wang and A.H. Zewail, Nature 364 (1993) 427.
[6] Ch. Lienau, J.C. Williamson and A.H. Zewail, Chem. Phys. Letters 213 (1993) 289.
[7] K.L. Cheng, W. Rosenberg, F.W. Wise, I.A. Walmsley and C.L. Tang, Appl. Phys. Letters 52 (1988) 519;
K. Kato, IEEE, J. Quantum Electron QE-22 (1986) 1013.
[8] J. Tellinghuisen, J. Chem. Phys. 82 (1985) 4012.
[9] P.B. Beeken, E.A. Hanson and G.W. Flynn, J. Chem. Phys. 78 (1983) 5892.
[10] R. Bohling, J. Langen and U. Schurath, Chem. Phys. 130 (1989) 419.
[11] M. Macler and M. Heaven, Chem. Phys. 151 (1991) 219.
[12] J. Tellinghuisen, J. Mol. Spectry. 94 (1982) 231.
[13] X. Zheng, S. Fei, M. Heaven and J. Tellinghuisen, J. Chem. Phys. 96 (1992) 4877.
[14] X. Zheng, S. Fei, M. Heaven and J. Tellinghuisen, J. Mol. Spectry. 149 (1991) 399.
[15] J. Tellinghuisen, J. Can. Phys. 62 (1984) 1933.
[16] A. Borrmann, Z. Li and C.C. Martens, J. Chem. Phys. 98 (1993) 8514;
C.C. Martens, Z. Li and A. Borrmann, SPIE Proc. 1858 (1993) 305.
[17] R. Zadoyan, Z. Li, C.C. Martens and V.A. Apkarian, J. Chem. Phys., to be published.
[18] J.A. Beswick, R. Monot, J.M. Phillipoz and H.V.D. Bergh, J. Chem. Phys. 86 (1987) 3965.
[19] M.L. Burke and W. Klemperer, J. Chem. Phys. 98 (1993) 1797, and references therein.
[20] I.H. Gersonde and H. Gabriel, J. Chem. Phys. 98 (1993) 2094.
[21] I. Benjamin, U. Banin and S. Ruhman, J. Chem. Phys. 98 (1993) 8337;
U. Banin and S. Ruhman, J. Chem. Phys. 98 (1993) 4391.
[22] D.A.V. Kliner, J.C. Alfano and P.F. Barbara, J. Chem. Phys. 98 (1993) 5375.
[23] A.H. Zewail, M. Dantus, R.M. Bowman and A. Mokhtari, J. Photochem. Photobiol. A 62 (1992) 301.
[24] B.J. Schwartz, J.C. King, J.Z. Zhang and C.B. Harris, Chem. Phys. Letters 203 (1993) 503, and references therein.
[25] C.L. Brooks and S.A. Adelman, J. Chem. Phys. 80 (1984) 5598, and references therein.